Available online at www.sciencedirect.com
SCIENCE DIRECT®
ELSEVIER
International Journal of Non-Linear Mechanics 39 (2004) 1093–1109
INTERNATIONAL JOURNAL OF NON-LINEAR MECHANICS
www.elsevier.com/locate/nlm

Finite deformation plate theory and large rigid-body motions

G.M. Kulikov*, S.V. Plotnikova

Department of Applied Mathematics and Mechanics, Tambov State Technical University, Sovetskaya Street, 106, Tambov 392000, Russia

Received 31 May 2002; received in revised form 30 March 2003; accepted 30 April 2003

Abstract

A refined non-linear first-order theory of multilayered anisotropic plates undergoing finite deformations is elaborated. The effects of the transverse shear and transverse normal strains, and laminated anisotropic material response are included. On the basis of this theory, a simple and efficient finite element model in conjunction with the total Lagrangian formulation and Newton–Raphson method is developed. The precise representation of large rigid-body motions in the displacement patterns of the proposed plate elements is also considered. This consideration requires the development of the strain–displacement equations of the finite deformation plate theory with regard to their consistency with the arbitrarily large rigid-body motions. The fundamental unknowns consist of six displacements and 11 strains of the face planes of the plate, and 11 stress resultants. The element characteristic arrays are obtained by using the Hu–Washizu mixed variational principle. To demonstrate the accuracy and efficiency of this formulation and compare its performance with other non-linear finite element models reported in the literature, extensive numerical studies are presented.

Keywords: Finite deformations; First-order multilayered plate theory; Large rigid-body motions; Finite-element method

1. Introduction

One of the main requirements of the modern plate theory that is intended for the general non-linear finite element (FE) formulation is that it must lead to strain-free modes for arbitrarily large rigid-body motions. The adequate representation of large rigid-body motions is a necessary condition if a non-linear element is to have the good accuracy and convergence properties. Therefore, when an inconsistent non-linear plate theory is used to construct any finite element, erroneous straining modes under arbitrarily large rigid-body motions may be appeared. This problem has been studied for the geometrically linear Kirchhoff–Love shell theory [1] and first-order shell theory [2,3] based on the Reissner–Mindlin kinematics (see e.g. [4,5]).

Herein, the more general study on the basis of the finite deformation first-order multilayered plate theory taking into account the transverse normal deformation response and bending–extension coupling is considered. As unknown functions six displacements of the face planes of the plate are chosen [6–9]. Such choice of displacements gives the possibility to deduce non-linear strain–displacement relationships,

* Corresponding author. Fax: +7-075-271-0216.
E-mail address: kulikov@apmath.tstu.ru (G.M. Kulikov).
URL: http://apm.tstu.ru/kulikov

0020-7462/$ - see front matter © 2003 Elsevier Ltd. All rights reserved.
doi:10.1016/S0020-7462(03)00099-4

which are objective, i.e., invariant under all rigid-body motions. It should be mentioned that in some works ([10,11] among others), developing the degenerate solid shell concept, displacement vectors of the face surfaces are also used. But in our first-order plate theory selecting as unknowns the displacements of the face planes has a principally another mechanical sense and allows one to deduce non-linear strain–displacement relationships with aforementioned attractive properties. In particular, such choice of unknowns permits special loading conditions at the face planes and plate edges to be accounted for.

Using the traditional non-linear Reissner–Mindlin theory in FE formulations for plates and shells is well established and has been shown to give acceptable results [12–19]. These formulations have the advantage that displacement and rotation trial functions may be used and these functions need only to be C^0 continuous. The developed FE formulation has the essential advantage, since only trial functions of displacements of the face planes may be used [2,3,8,9]. Moreover, our formulation is free of assumptions of small displacements, small rotations, small strains and small loading steps because herein the *exact* plate theory based on the fully non-linear strain–displacement relationships is discussed.

The FE formulation is based on a simple and efficient approximation of Reissner–Mindlin plates and shells via quadrilateral 4-node elements developed by Hughes and Tezduyar [20], and Wempner et al. [21]. The fundamental unknowns consist of six displacements and 11 strains of the face planes of the plate, and 11 stress resultants. The simplest admissible approximations of the 2-D fields are used, namely, bilinear approximations of the displacements, and assumed approximations of the strains and stress resultants. Additionally, in order to overcome the so-called Poisson thickness-locking [22–24] modified stress–strain relationships [6–9] are applied. As a result, no enhanced strains [13,14,22,23] are needed to obtain the computationally exact solutions of the bending dominated plate problems when Poisson's ratios are not zero.

The numerical results are presented to demonstrate the efficiency and high accuracy of the developed formulation and compare it with other FE formulations reported in the literature. For this purpose five tests are employed.

2. Strain–displacement relationships

Let us consider a plate of uniform thickness h. The plate may be defined as a 3-D body bounded by two bounding planes S^- and S^+, located at the distances δ^- and δ^+ measured with respect to the reference plane S, and the edge boundary cylindrical surface Ω that is perpendicular to the reference plane. Let the reference plane S be referred to the Cartesian coordinate system x_1 and x_2. The x_3-axis is oriented along the normal direction. The initial configuration of the plate is shown in Fig. 1(a) while Fig. 1(b) illustrates the final configuration.

The components of the Green–Lagrange strain tensor for finite strains can be written in a vector form as

$$2\varepsilon_{ij}^{\mathrm{e}} = \mathbf{u}_{,i}\mathbf{e}_j + \mathbf{u}_{,j}\mathbf{e}_i + \mathbf{u}_{,i}\mathbf{u}_{,j}, \tag{1a}$$

$$\mathbf{u} = \sum_i u_i \mathbf{e}_i, \tag{1b}$$

where $\mathbf{u}$ is the displacement vector; $u_i(x_1, x_2, x_3)$ are the components of this vector, which are always measured in accordance with the total Lagrangian formulation from the initial configuration to the final configuration directly (see Fig. 1); $\mathbf{e}_i$ are the unit base vectors. Here and in the following developments, the abbreviation $()_{,i}$ implies the partial derivative with respect to the coordinate x_i and Latin indices i, j, ℓ, m take the values 1, 2 and 3.

The finite deformation first-order plate theory is based on the linear approximation of displacements in the thickness direction [6–9]

$$\mathbf{u} = N^-(x_3)\,\mathbf{v}^- + N^+(x_3)\mathbf{v}^+, \tag{2a}$$

$$\mathbf{v}^{\pm} = \sum_i v_i^{\pm}\mathbf{e}_i, \tag{2b}$$

$$N^-(x_3) = \frac{1}{h}(\delta^+ - x_3), \quad N^+(x_3) = \frac{1}{h}(x_3 - \delta^-), \tag{2c}$$

where $\mathbf{v}^{\pm}$ are the displacement vectors of the face planes $S^{\pm}$; $v_i^{\pm}(x_1, x_2)$ are the displacements of the planes $S^{\pm}$; $N^{\pm}(x_3)$ are the linear shape functions. The advantage of the proposed approach is apparent, since using face displacements $v_i^{\pm}$ the kinematic boundary conditions at the face planes of the plate may be formulated. Moreover, this simplifies a formulation of

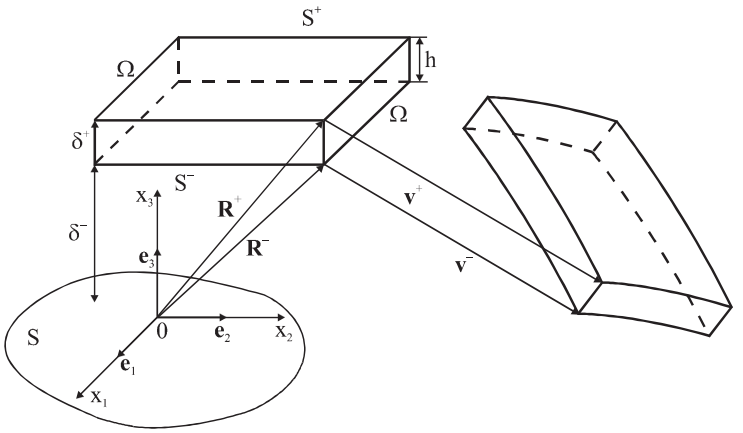

Fig. 1. Plate element: (a) initial configuration and (b) final configuration.

new FE models and provides a convenient way to express the non-linear strain–displacement relationships in terms of face plane strains.

Substituting displacements (2) into strain–displacement relationships (1), one can obtain the strain–displacement relationships of the finite deformation first-order theory of *moderately thick* plates

$$
\begin{aligned}
2\varepsilon^{\mathrm{a}}_{\alpha\beta} &= [N^-(x_3)\mathbf{v}^-_{,\alpha} + N^+(x_3)\mathbf{v}^+_{,\alpha}]\mathbf{e}_\beta \\
&\quad + [N^-(x_3)\mathbf{v}^-_{,\beta} + N^+(x_3)\mathbf{v}^+_{,\beta}]\mathbf{e}_\alpha \\
&\quad + [N^-(x_3)\mathbf{v}^-_{,\alpha} + N^+(x_3)\mathbf{v}^+_{,\alpha}][N^-(x_3)\mathbf{v}^-_{,\beta} \\
&\quad + N^+(x_3)\mathbf{v}^+_{,\beta}], \\
2\varepsilon^{\mathrm{a}}_{\alpha 3} &= N^-(x_3)(\boldsymbol{\beta}\mathbf{e}_\alpha + \mathbf{v}^-_{,\alpha}\mathbf{e}_3 + \boldsymbol{\beta}\mathbf{v}^-_{,\alpha}) \\
&\quad + N^+(x_3)(\boldsymbol{\beta}\mathbf{e}_\alpha + \mathbf{v}^+_{,\alpha}\mathbf{e}_3 + \boldsymbol{\beta}\mathbf{v}^+_{,\alpha}), \\
\varepsilon^{\mathrm{a}}_{33} &= \boldsymbol{\beta}\left(\mathbf{e}_3 + \tfrac{1}{2}\boldsymbol{\beta}\right), \qquad \boldsymbol{\beta} = \tfrac{1}{h}(\mathbf{v}^+ - \mathbf{v}^-).
\end{aligned} \tag{3}
$$

Throughout this paper greek indices $\alpha, \beta, \gamma, \delta$ take the values 1 and 2.

Strain–displacement relationships (3) are very attractive because they are objective, i.e., invariant under arbitrarily large rigid-body motions. It will be shown in Section 4. Note also that in-plane strains $\varepsilon^{\mathrm{a}}_{\alpha\beta}$ are distributed over the plate thickness according to the quadratic law. Taking into account that a plate has a moderate thickness, this complication of our finite deformation plate theory would be unreasonable because of the minor significance of the quadratic terms in most problems.

Therefore, more convenient strain–displacement relationships of the finite deformation first-order plate theory can be written as

$$
\begin{aligned}
\varepsilon^{\mathrm{b}}_{\alpha\beta} &= N^-(x_3)\mathscr{E}^-_{\alpha\beta} + N^+(x_3)\mathscr{E}^+_{\alpha\beta}, \\
\varepsilon^{\mathrm{b}}_{\alpha 3} &= N^-(x_3)\mathscr{E}^-_{\alpha 3} + N^+(x_3)\mathscr{E}^+_{\alpha 3}, \\
\varepsilon^{\mathrm{b}}_{33} &= \mathscr{E}_{33},
\end{aligned} \tag{4a}
$$

where $\mathscr{E}^\pm_{\alpha\beta}$ and $\mathscr{E}^\pm_{\alpha 3}$ are the in-plane and transverse shear strains of the face planes $S^\pm$ defined by

$$
\begin{aligned}
2\mathscr{E}^\pm_{\alpha\beta} &= \mathbf{v}^\pm_{,\alpha}\mathbf{e}_\beta + \mathbf{v}^\pm_{,\beta}\mathbf{e}_\alpha + \mathbf{v}^\pm_{,\alpha}\mathbf{v}^\pm_{,\beta}, \\
2\mathscr{E}^\pm_{\alpha 3} &= \boldsymbol{\beta}\mathbf{e}_\alpha + \mathbf{v}^\pm_{,\alpha}\mathbf{e}_3 + \boldsymbol{\beta}\mathbf{v}^\pm_{,\alpha}, \mathscr{E}_{33} = \boldsymbol{\beta}(\mathbf{e}_3 + \tfrac{1}{2}\boldsymbol{\beta}).
\end{aligned} \tag{4b}
$$

Strain–displacement relationships (4) are also objective. It will be discussed in Section 4.

Remark 2.1. The components of Green–Lagrange strain tensors (3) and (4) satisfy the first type of coupling conditions

$$
\varepsilon^{\mathrm{a}}_{\alpha\beta}(\delta^\pm) = \varepsilon^{\mathrm{b}}_{\alpha\beta}(\delta^\pm) = \mathscr{E}^\pm_{\alpha\beta}. \tag{5}
$$

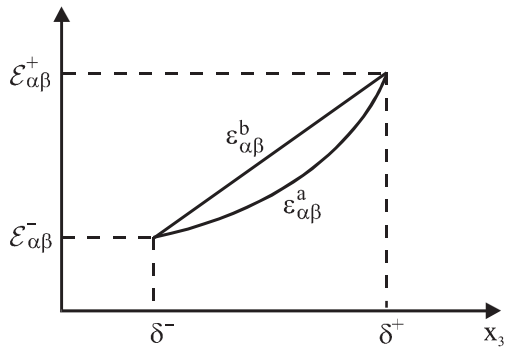

Fig. 2. Distribution of in-plane strains over the plate thickness.

This is illustrated in Fig. 2.

Remark 2.2. The components of Green–Lagrange strain tensor (4) as well as strain tensor (3) satisfy the second type of coupling conditions

$$2(\mathscr{E}^{+}_{\alpha 3} - \mathscr{E}^{-}_{\alpha 3}) = h\mathscr{E}_{33,\alpha}. \tag{6}$$

This is due to the equation

$$2(\mathscr{E}^{+}_{\alpha 3} - \mathscr{E}^{-}_{\alpha 3}) = h\boldsymbol{\beta}_{,\alpha}(\mathbf{e}_3 + \boldsymbol{\beta}),$$

which immediately follows from relations (4b). Coupling conditions (6) play a central role in our FE formulation (see Section 7).

For the FE implementation of strain–displacement relationships (4) they need to be written in the scalar form

$$\mathscr{E}^{\pm}_{\alpha\beta} = e^{\pm}_{\alpha\beta} + \eta^{\pm}_{\alpha\beta}, \quad \mathscr{E}^{\pm}_{\alpha 3} = e^{\pm}_{\alpha 3} + \eta^{\pm}_{\alpha 3}, \quad \mathscr{E}_{33} = e_{33} + \eta_{33}, \tag{7a}$$

$$2e^{\pm}_{\alpha\beta} = v^{\pm}_{\alpha,\beta} + v^{\pm}_{\beta,\alpha}, \quad 2e^{\pm}_{\alpha 3} = \beta_\alpha + v^{\pm}_{3,\alpha}, \quad e_{33} = \beta_3, \tag{7b}$$

$$2\eta^{\pm}_{\alpha\beta} = \sum_i v^{\pm}_{i,\alpha} v^{\pm}_{i,\beta}, \quad 2\eta^{\pm}_{\alpha 3} = \sum_i \beta_i v^{\pm}_{i,\alpha}, \quad 2\eta_{33} = \sum_i \beta_i^2, \tag{7c}$$

$$\beta_i = \frac{1}{h}(v_i^{+} - v_i^{-}). \tag{7d}$$

3. Classical strain–displacement relationships

The traditional finite deformation Reissner–Mindlin plate theory is based on the classical kinematic hypothesis adopted for the displacement vector

$$\mathbf{u} = \mathbf{v} + x_3\boldsymbol{\beta}, \tag{8a}$$

where $\mathbf{v}$ is the displacement vector; $\boldsymbol{\beta}$ is the rotation vector defined by

$$\mathbf{v} = \frac{\delta^{+}}{h}\mathbf{v}^{-} - \frac{\delta^{-}}{h}\mathbf{v}^{+}, \quad \boldsymbol{\beta} = \frac{1}{h}(\mathbf{v}^{+} - \mathbf{v}^{-}). \tag{8b}$$

Substituting displacement (8a) into strain–displacement relationships (1) and allowing for Eq. (8b), one may obtain

$$2\varepsilon^{c}_{\gamma\delta} = \mathbf{v}_{,\gamma}\mathbf{e}_\delta + \mathbf{v}_{,\delta}\mathbf{e}_\gamma + \mathbf{v}_{,\gamma}\mathbf{v}_{,\delta} + x_3(\boldsymbol{\beta}_{,\gamma}\mathbf{e}_\delta + \boldsymbol{\beta}_{,\delta}\mathbf{e}_\gamma + \mathbf{v}_{,\gamma}\boldsymbol{\beta}_{,\delta} + \mathbf{v}_{,\delta}\boldsymbol{\beta}_{,\gamma}) + x_3^2\boldsymbol{\beta}_{,\gamma}\boldsymbol{\beta}_{,\delta},$$

$$2\varepsilon^{c}_{\gamma 3} = \boldsymbol{\beta}\mathbf{e}_\gamma + \mathbf{v}_{,\gamma}(\mathbf{e}_3 + \boldsymbol{\beta}) + x_3\boldsymbol{\beta}_{,\gamma}(\mathbf{e}_3 + \boldsymbol{\beta}),$$

$$\varepsilon^{c}_{33} = \boldsymbol{\beta}(\mathbf{e}_3 + \tfrac{1}{2}\boldsymbol{\beta}). \tag{9}$$

It will be proved in the next section that strain–displacement relationships (9) are also invariant under large rigid-body motions.

4. Large rigid-body motions

An arbitrarily large rigid-body motion can be defined as

$$\mathbf{u}^{R} = \boldsymbol{\Delta} + (\mathbf{A} - \mathbf{E})\mathbf{R}, \tag{10a}$$

$$\mathbf{R} = \sum_i x_i\mathbf{e}_i, \qquad \boldsymbol{\Delta} = \sum_i \Delta_i\mathbf{e}_i, \tag{10b}$$

where $\mathbf{R}$ is the position vector of any point of the plate; $\boldsymbol{\Delta}$ is the constant displacement (translation) vector; $\mathbf{E}$ is the identity matrix; $\mathbf{A}$ is the orthogonal rotation matrix. In particular, rigid-body motions of the face planes are

$$\mathbf{v}^{\pm R} = \boldsymbol{\Delta} + (\mathbf{A} - \mathbf{E})\mathbf{R}^{\pm}, \tag{11a}$$

$$\mathbf{R}^{\pm} = \sum_\alpha x_\alpha\mathbf{e}_\alpha + \delta^{\pm}\mathbf{e}_3, \tag{11b}$$

where $\mathbf{R}^{\pm}$ are the position vectors of points of the top and bottom planes $S^{\pm}$.

The derivatives of the translation vector and position vectors of the face planes with respect to the coordinate x_α can be written as

$$\mathbf{\Delta}_{,\alpha} = \mathbf{0}, \qquad \mathbf{R}^{\pm}_{,\alpha} = \mathbf{e}_\alpha. \tag{12}$$

Taking into account Eqs. (11) and (12), one can obtain the following expression for the derivatives:

$$\mathbf{v}^{\pm R}_{,\alpha} = \mathbf{A}\mathbf{e}_\alpha - \mathbf{e}_\alpha, \qquad \boldsymbol{\beta}^{R}_{,\alpha} = \mathbf{0}. \tag{13}$$

It can be verified by using Eqs. (11) and (13) that strains from Eqs. (3) and (4) are all zero in a general large rigid-body motion, i.e.,

$$2\varepsilon^{aR}_{ij} = (\mathbf{A}\mathbf{e}_i)(\mathbf{A}\mathbf{e}_j) - \mathbf{e}_i\mathbf{e}_j = 0, \tag{14a}$$

$$2\varepsilon^{bR}_{ij} = (\mathbf{A}\mathbf{e}_i)(\mathbf{A}\mathbf{e}_j) - \mathbf{e}_i\mathbf{e}_j = 0. \tag{14b}$$

This conclusion is true because an orthogonal transformation retains the scalar product of the vectors. So, our modified strains (3) and (4) are objective, i.e., invariant under arbitrarily large rigid-body motions.

It can be also verified applying Eqs. (11) and (13) that classical strains (9) are all zero in a large rigid-body motion because

$$2\varepsilon^{cR}_{ij} = (\mathbf{A}\mathbf{e}_i)(\mathbf{A}\mathbf{e}_j) - \mathbf{e}_i\mathbf{e}_j = 0. \tag{15}$$

5. Stress–strain equations

Consider first an orthotropic plate whose axes of material symmetry x'_1 and x'_2 do not coincide with coordinate directions x_1 and x_2. In axes of material symmetry x'_1, x'_2 and x_3, the equations of the complete 3-D Hooke's law will be

$$\varepsilon_{1'1'} = \frac{1}{E_1} S_{1'1'} - \frac{\nu_{21}}{E_2} S_{2'2'} - \frac{\nu_{31}}{E_3} S_{33},$$

$$\varepsilon_{2'2'} = -\frac{\nu_{12}}{E_1} S_{1'1'} + \frac{1}{E_2} S_{2'2'} - \frac{\nu_{32}}{E_3} S_{33}, \tag{16a}$$

$$\varepsilon_{33} = -\frac{\nu_{13}}{E_1} S_{1'1'} - \frac{\nu_{23}}{E_2} S_{2'2'} + \frac{1}{E_3} S_{33}, \tag{16b}$$

$$2\varepsilon_{1'2'} = \frac{1}{G_{12}} S_{1'2'}, \quad 2\varepsilon_{1'3} = \frac{1}{G_{13}} S_{1'3},$$

$$2\varepsilon_{2'3} = \frac{1}{G_{23}} S_{2'3}, \tag{16c}$$

where $S_{1'1'}, S_{2'2'}, S_{33}$ and $S_{1'2'}, S_{1'3}, S_{2'3}$ are the normal and shear components of the second Piola–Kirchhoff stress tensor in the x'_1, x'_2, x_3 coordinate system; E_1, E_2 and E_3 are the elastic moduli; G_{12}, G_{13} and G_{23} are the shear moduli; ν_{ij} are Poisson's ratios. From reasons of symmetry, we have

$$\nu_{ij}E_j = \nu_{ji}E_i \quad \text{for } i \neq j.$$

Solving Eqs. (16a) and (16b) for the normal stresses, one may find

$$S_{1'1'} = Q_{11}\varepsilon_{1'1'} + Q_{12}\varepsilon_{2'2'} + Q_{13}\varepsilon_{33},$$

$$S_{2'2'} = Q_{21}\varepsilon_{1'1'} + Q_{22}\varepsilon_{2'2'} + Q_{23}\varepsilon_{33},$$

$$S_{33} = Q_{31}\varepsilon_{1'1'} + Q_{32}\varepsilon_{2'2'} + Q_{33}\varepsilon_{33}, \tag{17}$$

where $[Q_{ij}]$ is the symmetric material matrix, which components are defined as

$$Q_{11} = \frac{1}{\Delta}(1 - \nu_{23}\nu_{32})E_1, \quad Q_{22} = \frac{1}{\Delta}(1 - \nu_{13}\nu_{31})E_2,$$

$$Q_{33} = \frac{1}{\Delta}(1 - \nu_{12}\nu_{21})E_3,$$

$$Q_{12} = \frac{1}{\Delta}(\nu_{12} + \nu_{13}\nu_{32})E_2,$$

$$Q_{21} = \frac{1}{\Delta}(\nu_{21} + \nu_{31}\nu_{23})E_1,$$

$$Q_{13} = \frac{1}{\Delta}(\nu_{31} + \nu_{21}\nu_{32})E_1,$$

$$Q_{31} = \frac{1}{\Delta}(\nu_{13} + \nu_{12}\nu_{23})E_3,$$

$$Q_{23} = \frac{1}{\Delta}(\nu_{32} + \nu_{12}\nu_{31})E_2,$$

$$Q_{32} = \frac{1}{\Delta}(\nu_{23} + \nu_{21}\nu_{13})E_3, \tag{18}$$

$$\Delta = 1 - \nu_{12}\nu_{21} - \nu_{13}\nu_{31} - \nu_{23}\nu_{32} - 2\nu_{12}\nu_{23}\nu_{31}.$$

Unfortunately, this formulation on the basis of the complete 3-D constitutive law (16c) and (17) is deficient because the so-called Poisson thickness locking [22–24] can occur. This phenomenon occurs in bending dominated plate problems when Poison's ratios are not equal to zero. The main reason is that Poisson's effect in the thickness direction is taken into account

in equations of Hooke's law for the normal in-plane strains (16a), i.e., Poisson's ratios ν_{31} and ν_{32} should be formally set to zero.

In order to avoid Poisson thickness locking, we invoke the standard engineering assumption

$$S_{33} \ll S_{1'1'} \quad \text{and} \quad S_{33} \ll S_{2'2'}.$$

Allowing for this assumption into Eq. (16a) and solving for the normal in-plane stresses, one obtains

$$\begin{aligned} S_{1'1'} &= Q_{11}\varepsilon_{1'1'} + Q_{12}\varepsilon_{2'2'}, \\ S_{2'2'} &= Q_{21}\varepsilon_{1'1'} + Q_{22}\varepsilon_{2'2'}, \end{aligned} \tag{19}$$

where

$$\begin{aligned} &Q_{11} = \frac{1}{d}E_1, \quad Q_{22} = \frac{1}{d}E_2, \quad Q_{12} = \frac{1}{d}\nu_{12}E_2, \\ &Q_{21} = \frac{1}{d}\nu_{21}E_1, \quad Q_{13} = 0, \quad Q_{23} = 0, \\ &d = 1 - \nu_{12}\nu_{21}. \end{aligned} \tag{20}$$

Substituting further stresses (19) in Eq. (16b) and solving for the transverse normal stress, we arrive at the following formula [7,25]:

$$S_{33} = Q_{31}\varepsilon_{1'1'} + Q_{32}\varepsilon_{2'2'} + Q_{33}\varepsilon_{33}, \tag{21}$$

where

$$\begin{aligned} &Q_{31} = \frac{1}{d}(\nu_{13} + \nu_{12}\nu_{23})E_3, \\ &Q_{32} = \frac{1}{d}(\nu_{23} + \nu_{21}\nu_{13})E_3, \quad Q_{33} = E_3. \end{aligned} \tag{22}$$

Remark 5.1. A comparison of Eq. (18) with Eqs. (20) and (22) shows that the corresponding expressions are exactly the same when Poisson's ratios $\nu_{31}=0$ and $\nu_{32}=0$. This partially substantiates our modification of the 3-D constitutive law.

In coordinate directions x_1, x_2 and x_3, when a case of monoclinic symmetry is realized, the equations of the complete constitutive law as well as the modified constitutive law can be represented in the more general form

$$S_{ij} = \sum_{\ell,m} C_{ij\ell m}\varepsilon_{\ell m}, \tag{23}$$

where $C_{ij\ell m}$ are the components of the elasticity tensor defined by

$$\begin{aligned} &C_{1111} = c^4Q_{11} + 2c^2s^2\Theta + s^4Q_{22}, \\ &C_{1122} = c^2s^2(Q_{11} + Q_{22} - 2\Theta) + Q_{12}, \\ &C_{1133} = c^2Q_{13} + s^2Q_{23}, \\ &C_{1112} = c^3s(\Theta - Q_{11}) + cs^3(Q_{22} - \Theta), \\ &C_{2211} = C_{1122}, \quad C_{2222} = s^4Q_{11} + 2c^2s^2\Theta + c^4Q_{22}, \\ &C_{2233} = s^2Q_{13} + c^2Q_{23}, \\ &C_{2212} = cs^3(\Theta - Q_{11}) + c^3s(Q_{22} - \Theta), \\ &C_{3311} = c^2Q_{31} + s^2Q_{32}, \\ &C_{3322} = s^2Q_{31} + c^2Q_{32}, \quad C_{3333} = Q_{33}, \\ &C_{3312} = cs(Q_{32} - Q_{31}), \quad C_{1211} = C_{1112}, \\ &C_{1222} = C_{2212}, \\ &C_{1233} = cs(Q_{23} - Q_{13}), \\ &C_{1212} = c^2s^2(Q_{11} + Q_{22} - 2\Theta) + G_{12}, \\ &C_{1313} = c^2G_{13} + s^2G_{23}, \quad C_{1323} = cs(G_{23} - G_{13}), \\ &C_{2313} = C_{1323}, \\ &C_{2323} = s^2G_{13} + c^2G_{23}, \quad C_{ij\ell m} = C_{ijm\ell}, \\ &C_{ij\ell m} = C_{ji\ell m}, \\ &\Theta = Q_{12} + 2G_{12} = Q_{21} + 2G_{12}, \quad c = \cos\varphi, \\ &s = \sin\varphi. \end{aligned} \tag{24}$$

Here, φ is the angle between axes of material symmetry and coordinate directions x_1 and x_2; and all components of the elasticity tensor not explicitly written are considered to be equal to zero. It is apparent that using relations $Q_{13}=0$ and $Q_{23}=0$ into Eq. (24) yields the modified constitutive law, since

$$C_{1133} = C_{2233} = C_{1233} = 0, \tag{25}$$

i.e., Poisson's effect in the thickness direction is not taken into account in constitutive equations (23) for the in-plane stresses $S_{\alpha\beta}$.

It should be mentioned that the proposed approach gives the possibility to use six-parameter plate model in conjunction with the assumed strain method

without additional stabilization procedures. No enhanced strains [13,14,22,23] are needed to obtain the solution of bending dominated plate problems, and no Poisson thickness locking can occur when Poisson's ratios are not equal to zero. It will be discussed in Section 8.

6. Hu–Washizu variational equation for multilayered anisotropic plate

Let us consider a plate built up in the general case by the arbitrary superposition across the thickness of N layers of uniform thickness h_k. The kth layer may be defined as a 3-D body bounded by two planes S_{k-1} and S_k, located at the distances δ_{k-1} and δ_k measured with respect to the reference plane S, and the edge boundary cylindrical surface Ω_k that is perpendicular to the planes S_{k-1} and S_k (see Fig. 3). Let the reference plane S be referred to the Cartesian coordinates x_1 and x_2. The x_3 axis is oriented along the normal direction.

The constituent layers of the plate are supposed to be rigidly joined, so that no slip on contact planes and no separation of layers can occur. The material of each constituent layer is assumed to be linearly elastic and anisotropic. Let p_i^- and p_i^+ be the intensities of the external loading acting on the bottom plane $S^- = S_0$ and the top plane $S^+ = S_N$ in the x_i coordinate directions, respectively, while $\mathbf{q}^{(k)} = q_\nu^{(k)}\boldsymbol{\nu} + q_t^{(k)}\mathbf{t} + q_3^{(k)}\mathbf{e}_3$ be the external loading vector acting on the edge boundary surface Ω_k, where $q_\nu^{(k)}$, $q_t^{(k)}$ and $q_3^{(k)}$ are the components of its vector in the ν, t and x_3 directions; $\boldsymbol{\nu}$ and $\mathbf{t}$ are the normal and tangential unit vectors to the bounding curve Γ (see Fig. 3). Here and in the following developments the index $k = \overline{1, N}$ identifies the belonging of any quantity to the kth layer.

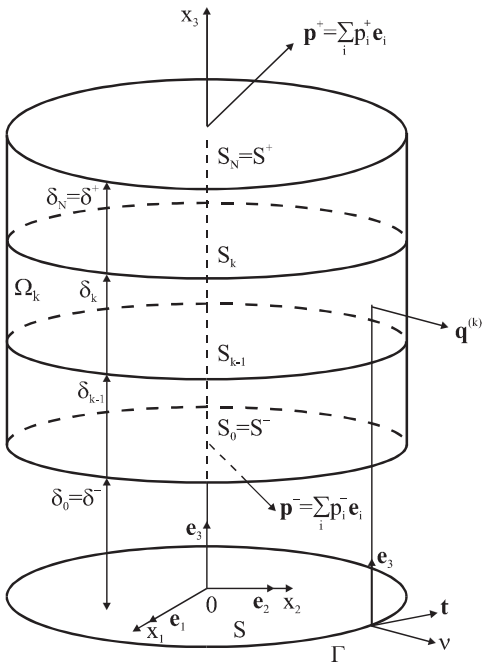

Fig. 3. Multilayered plate.

The Hu–Washizu 3-D variational principle [26] for the multilayered anisotropic plate can be written in the following form:

$$\int_S \int \sum_k \int_{\delta_{k-1}}^{\delta_k} \sum_{i,j} \left[\left(S_{ij}^{(k)} - \sum_{\ell,m} C_{ij\ell m}^{(k)} \varepsilon_{\ell m} \right) \times \delta\varepsilon_{ij} + (\varepsilon_{ij} - \varepsilon_{ij}^u)\,\delta S_{ij}^{(k)} - S_{ij}^{(k)} \delta\varepsilon_{ij}^u \right] \mathrm{d}x_3\,\mathrm{d}S + \int_{S^+} \int \sum_i p_i^+ \delta u_i\,\mathrm{d}S - \int_{S^-} \int \sum_i p_i^- \delta u_i\,\mathrm{d}S + \oint_\Gamma \sum_k \int_{\delta_{k-1}}^{\delta_k} (q_\nu^{(k)} \delta u_\nu + q_t^{(k)} \delta u_t + q_3^{(k)} \delta u_3)\,\mathrm{d}x_3 \mathrm{d}s = 0, \tag{26}$$

where ε_{ij}^u are the strains due to the displacement field; ε_{ij} are the independently assumed strains; u_ν, u_t and u_3 are the components of the displacement vector in the coordinate system ν, t and x_3 (see Fig. 3).

The finite deformation first-order theory of multilayered anisotropic plates is based on the linear approximation of the displacement vector in thickness direction (2), where we should set $\delta^- = \delta_0$ and $\delta^+ = \delta_N$. Substituting *independent* approximations of displacements (2) and strains

$$\begin{aligned} \varepsilon_{\alpha\beta} &= N^-(x_3) E_{\alpha\beta}^- + N^+(x_3) E_{\alpha\beta}^+, \\ \varepsilon_{\alpha 3} &= N^-(x_3) E_{\alpha 3}^- + N^+(x_3) E_{\alpha 3}^+, \\ \varepsilon_{33} &= E_{33} \end{aligned} \tag{27}$$

into variational equation (26), and allowing for strain–displacement relationships (4) and (7), one can obtain

$$\int_S \int \Bigg(\sum_{i+j<6} \Bigg\{ \Bigg[T_{ij}^- - \sum_{\ell+m<6} \left(D_{ij\ell m}^{00} E_{\ell m}^- + D_{ij\ell m}^{01} E_{\ell m}^+ \right) - D_{ij33}^- E_{33} \Bigg] \delta E_{ij}^- + \Bigg[T_{ij}^+ - \sum_{\ell+m<6} \left(D_{ij\ell m}^{01} E_{\ell m}^- + D_{ij\ell m}^{11} E_{\ell m}^+ \right) - D_{ij33}^+ E_{33} \Bigg] \delta E_{ij}^+ + (E_{ij}^- - e_{ij}^- - \eta_{ij}^-)\,\delta T_{ij}^- + (E_{ij}^+ - e_{ij}^+ - \eta_{ij}^+)\,\delta T_{ij}^+ - T_{ij}^-(\delta e_{ij}^- + \delta \eta_{ij}^-) - T_{ij}^+(\delta e_{ij}^+ + \delta \eta_{ij}^+) \Bigg\} + \Bigg[T_{33} - \sum_{\ell+m<6} \left(D_{33\ell m}^- E_{\ell m}^- + D_{33\ell m}^+ E_{\ell m}^+ \right) - D_{3333} E_{33} \Bigg] \delta E_{33} + (E_{33} - e_{33} - \eta_{33}) \delta T_{33} - T_{33}(\delta e_{33} + \delta \eta_{33}) + \sum_i \left(p_i^+ \delta v_i^+ - p_i^- \delta v_i^- \right) \Bigg) \mathrm{d}S + \oint_\Gamma \left(\hat{T}_{vv}^- \delta v_v^- + \hat{T}_{vv}^+ \delta v_v^+ + \hat{T}_{vt}^- \delta v_t^- + \hat{T}_{vt}^+ \delta v_t^+ + \hat{T}_{v3}^- \delta v_3^- + \hat{T}_{v3}^+ \delta v_3^+ \right) \mathrm{d}s = 0, \tag{28}$$

where $v_v^\pm$, $v_t^\pm$ and $v_3^\pm$ are the components of the displacement vectors of the face planes $S^\pm$ in the coordinate system v, t and x_3; $T_{\alpha i}^\pm$ and T_{33} are the stress resultants; $\hat{T}_{vv}^\pm$, $\hat{T}_{vt}^\pm$ and $\hat{T}_{v3}^\pm$ are the external load resultants; $D_{ij\ell m}^{pq}$ are the components of the through-the-thickness elasticity tensors, which are defined as

$$D_{ij\ell m}^{pq} = \sum_k \int_{\delta_{k-1}}^{\delta_k} C_{ij\ell m}^{(k)} [N^-(x_3)]^{2-p-q} \times [N^+(x_3)]^{p+q}\,\mathrm{d}x_3 \quad (p,q=0,1),$$

$$D_{ij33}^- = D_{ij33}^{00} + D_{ij33}^{01}, \quad D_{ij33}^+ = D_{ij33}^{01} + D_{ij33}^{11},$$

$$D_{3333} = D_{3333}^- + D_{3333}^+, \tag{29a}$$

$$T_{\alpha i}^\pm = \sum_k \int_{\delta_{k-1}}^{\delta_k} S_{\alpha i}^{(k)} N^\pm(x_3)\,\mathrm{d}x_3,$$

$$T_{33} = \sum_k \int_{\delta_{k-1}}^{\delta_k} S_{33}^{(k)}\,\mathrm{d}x_3,$$

$$\hat{T}_{v\text{æ}}^\pm = \sum_k \int_{\delta_{k-1}}^{\delta_k} q_{\text{æ}}^{(k)} N^\pm(x_3)\,\mathrm{d}x_3 \quad (\text{æ} = v,t,3). \tag{29b}$$

Variational equation (28) provides a foundation for the FE formulation for finite deformation plates on the basis of the above constitutive laws, namely, complete when $D_{\alpha\beta 33}^\pm \neq 0$, and modified when in accordance with Eq. (25) $D_{\alpha\beta 33}^\pm = 0$. As we remember, conditions $D_{\alpha\beta\gamma 3}^{pq} = 0$ and $D_{\alpha 333}^{pq} = 0$ are also fulfilled.

7. FE formulation

Variational equation (28) for the plate element can be written in a matrix form as

$$\int_{-1}^{1} \int_{-1}^{1} [(\mathbf{T} - \mathbf{DE})^{\mathrm{T}} \delta \mathbf{E} + (\mathbf{E} - \mathbf{e} - \boldsymbol{\eta})^{\mathrm{T}} \delta \mathbf{T} - \mathbf{T}^{\mathrm{T}} (\delta \mathbf{e} + \delta \boldsymbol{\eta}) + \mathbf{P}^{\mathrm{T}} \delta \mathbf{v}]\,\mathrm{d}\xi_1\,\mathrm{d}\xi_2 + \oint_{\Gamma^{e\ell}} \hat{\mathbf{T}}_\Gamma^{\mathrm{T}} \delta \mathbf{v}_\Gamma\,\mathrm{d}s = 0,$$

$$\mathbf{v} = [v_1^-\ v_1^+\ v_2^-\ v_2^+\ v_3^-\ v_3^+]^{\mathrm{T}},$$

$$\mathbf{v}_\Gamma = [v_v^-\ v_v^+\ v_t^-\ v_t^+\ v_3^-\ v_3^+]^{\mathrm{T}},$$

$$\mathbf{E} = [E_{11}^- E_{11}^+ E_{22}^- E_{22}^+ 2E_{12}^- 2E_{12}^+ 2E_{13}^- 2E_{13}^+ 2E_{23}^- 2E_{23}^+ E_{33}]^{\mathrm{T}},$$

$$\mathbf{e} = [e_{11}^- e_{11}^+ e_{22}^- e_{22}^+ 2e_{12}^- 2e_{12}^+ 2e_{13}^- 2e_{13}^+ 2e_{23}^- 2e_{23}^+ e_{33}]^{\mathrm{T}},$$

$$\boldsymbol{\eta} = [\eta_{11}^- \eta_{11}^+ \eta_{22}^- \eta_{22}^+ 2\eta_{12}^- 2\eta_{12}^+ 2\eta_{13}^- 2\eta_{13}^+ 2\eta_{23}^- 2\eta_{23}^+ \eta_{33}]^{\mathrm{T}},$$

$$\mathbf{T} = [T_{11}^- T_{11}^+ T_{22}^- T_{22}^+ T_{12}^- T_{12}^+ T_{13}^- T_{13}^+ T_{23}^- T_{23}^+ T_{33}]^{\mathrm{T}},$$

$$\hat{\mathbf{T}}_{\Gamma} = [\hat{T}_{vv}^- \hat{T}_{vv}^+ \hat{T}_{vt}^- \hat{T}_{vt}^+ \hat{T}_{v3}^- \hat{T}_{v3}^+]^{\mathrm{T}},$$

$$\mathbf{P} = [-p_1^- p_1^+ - p_2^- p_2^+ - p_3^- p_3^+]^{\mathrm{T}}, \tag{30}$$

where ξ_1 and ξ_2 are the local coordinates of the element; $\mathbf{v}$ is the displacement vector; $\mathbf{v}_{\Gamma}$ is the displacement vector of the element edge $\Gamma^{e\ell}$; $\mathbf{E}$ is the strain vector; $\mathbf{e}$ and $\boldsymbol{\eta}$ are the linear and non-linear parts of the strain–displacement transformation vector; $\mathbf{T}$ is the stress resultant vector; $\hat{\mathbf{T}}_{\Gamma}$ is the loading resultant vector acting on the edge of the element; $\mathbf{P}$ is the surface traction vector; $\mathbf{D}$ is either the symmetric constitutive stiffness matrix of order 11×11, which components are defined by Eqs. (18), (24) and (29a), if one uses the 3-D complete constitutive law or the non-symmetric matrix, which components are defined by Eqs. (20), (22), (24) and (29a), in a case of applying the modified constitutive law.

For the simplest quadrilateral 4-node plate element, the displacement field is approximated according to the standard C^o interpolation

$$\mathbf{v} = \sum_r N_r \mathbf{v}_r, \tag{31}$$

where $\mathbf{v}_r = [v_{1r}^- v_{1r}^+ v_{2r}^- v_{2r}^+ v_{3r}^- v_{3r}^+]^{\mathrm{T}}$ are the displacement vectors of the element nodes; $N_r(\xi_1, \xi_2)$ are the linear shape functions of the element; the index r denotes a number of nodes and equals $\overline{1,4}$. The load vector is also assumed to vary linearly inside the element.

In accordance with the assumed strain concept developed by Hughes and Tezduyar [20], Wempner et al. [21], and Betsch and Stein [13], the following strain interpolations are adopted:

$$\mathbf{E} = \sum_{r_1,r_2} \mathbf{Q}^{r_1 r_2} \mathbf{E}^{r_1 r_2} \xi_1^{r_1} \xi_2^{r_2}. \tag{32}$$

Here,

$$\mathbf{E}^{00} = [E_{11}^{-00} E_{11}^{+00} E_{22}^{-00} E_{22}^{+00} 2E_{12}^{-00} 2E_{12}^{+00} 2E_{13}^{-00} 2E_{13}^{+00} 2E_{23}^{-00} 2E_{23}^{+00} E_{33}^{00}]^{\mathrm{T}},$$

$$\mathbf{E}^{01} = [E_{11}^{-01} E_{11}^{+01} 2E_{13}^{-01} 2E_{13}^{+01} E_{33}^{01}]^{\mathrm{T}},$$

$$\mathbf{E}^{10} = [E_{22}^{-10} E_{22}^{+10} 2E_{23}^{-10} 2E_{23}^{+10} E_{33}^{10}]^{\mathrm{T}}, \quad \mathbf{E}^{11} = [E_{33}^{11}],$$

$$\mathbf{Q}^{01} = \begin{bmatrix} 1&0&0&0&0\\ 0&1&0&0&0\\ 0&0&0&0&0\\ 0&0&0&0&0\\ 0&0&0&0&0\\ 0&0&0&0&0\\ 0&0&1&0&0\\ 0&0&0&1&0\\ 0&0&0&0&0\\ 0&0&0&0&0\\ 0&0&0&0&1 \end{bmatrix},$$

$$\mathbf{Q}^{10} = \begin{bmatrix} 0&0&0&0&0\\ 0&0&0&0&0\\ 1&0&0&0&0\\ 0&1&0&0&0\\ 0&0&0&0&0\\ 0&0&0&0&0\\ 0&0&0&0&0\\ 0&0&0&0&0\\ 0&0&1&0&0\\ 0&0&0&1&0\\ 0&0&0&0&1 \end{bmatrix},$$

$$\mathbf{Q}^{11} = \begin{bmatrix} 0 \\ 0 \\ 0 \\ 0 \\ 0 \\ 0 \\ 0 \\ 0 \\ 0 \\ 0 \\ 1 \end{bmatrix}, \tag{33}$$

where $\mathbf{Q}^{00}$ is the identity matrix of order 11×11; $\mathbf{E}^{00}$ is the vector of homogeneous states of strains; $\mathbf{E}^{01}$, $\mathbf{E}^{10}$ and $\mathbf{E}^{11}$ are the vectors of higher approximation modes of strains. Throughout this section superscripts r_1 and r_2 take the values 0 and 1.

The interpolations of the stress resultants follow the forms of the conjugate strains:

$$\mathbf{T} = \sum_{r_1,r_2} \mathbf{Q}^{r_1 r_2} \mathbf{T}^{r_1 r_2} \xi_1^{r_1} \xi_2^{r_2}, \tag{34}$$

where

$$\mathbf{T}^{00} = [T_{11}^{-00}\ T_{11}^{+00}\ T_{22}^{-00}\ T_{22}^{+00}\ T_{12}^{-00}\ T_{12}^{+00}\ T_{13}^{-00}\ T_{13}^{+00} T_{23}^{-00}\ T_{23}^{+00}\ T_{33}^{00}]^{\mathrm{T}},$$

$$\mathbf{T}^{01} = [T_{11}^{-01}\ T_{11}^{+01}\ T_{13}^{-01} T_{13}^{+01}\ T_{33}^{01}]^{\mathrm{T}},$$

$$\mathbf{T}^{10} = [T_{22}^{-10}\ T_{22}^{+10}\ T_{23}^{-10}\ T_{23}^{+10}\ T_{33}^{10}]^{\mathrm{T}},$$

$$\mathbf{T}^{11} = [T_{33}^{11}].$$

Accounting for strain–displacement relationships (7) and substituting Eqs. (31)–(34) into variational equation (30), one can obtain using the standard variational procedure governing equations of the present FE formulation

$$\mathbf{E}^{r_1 r_2} = (\mathbf{Q}^{r_1 r_2})^{\mathrm{T}} (\mathbf{B}^{r_1 r_2} + \mathbf{A}^{r_1 r_2} \mathbf{V}) \mathbf{V}, \tag{35a}$$

$$\mathbf{T}^{r_1 r_2} = (\mathbf{Q}^{r_1 r_2})^{\mathrm{T}} \mathbf{D} \mathbf{Q}^{r_1 r_2} \mathbf{E}^{r_1 r_2}, \tag{35b}$$

$$\sum_{r_1,r_2} \frac{1}{3^{r_1+r_2}} (\mathbf{B}^{r_1 r_2} + 2\mathbf{A}^{r_1 r_2} \mathbf{V})^{\mathrm{T}} \mathbf{Q}^{r_1 r_2} \mathbf{T}^{r_1 r_2} = \mathbf{F}, \tag{35c}$$

where $\mathbf{V} = [\mathbf{v}_1^{\mathrm{T}}\ \mathbf{v}_2^{\mathrm{T}}\ \mathbf{v}_3^{\mathrm{T}}\ \mathbf{v}_4^{\mathrm{T}}]^{\mathrm{T}}$ is the displacement vector at nodal points of the element; $\mathbf{F}$ is the force vector; $\mathbf{B}^{r_1 r_2}$ are the matrices of order 11×24 corresponding to the linear strain–displacement transformation; $\mathbf{A}^{r_1 r_2}$ are the 3-D arrays of order $11 \times 24 \times 24$ corresponding to the non-linear strain–displacement transformation. It is apparent that in Eqs. (35a) and (35c) $\mathbf{A}^{r_1 r_2} \mathbf{V}$ imply matrices of order 11×24, and the following rule is used in calculations:

$$(\mathbf{A}^{r_1 r_2} \mathbf{V})_{pq} = \sum_s A_{pqs}^{r_1 r_2} V_s$$

$$(p = \overline{1,11} \text{ and } q, s = \overline{1,24}).$$

Remark 7.1. The components of the assumed transverse shear and normal strains satisfy coupling conditions

$$hE_{33}^{10} = 2(E_{13}^{+00} - E_{13}^{-00}),$$

$$hE_{33}^{01} = 2(E_{23}^{+00} - E_{23}^{-00}),$$

$$hE_{33}^{11} = 2(E_{13}^{+01} - E_{13}^{-01}),$$

$$hE_{33}^{11} = 2(E_{23}^{+10} - E_{23}^{-10}), \tag{36}$$

which immediately follow from elemental equilibrium equations (35a) and have a form of corresponding coupling conditions (6) for strains due to the displacement field.

Relationships (36) imply that only seven higher approximation modes of the assumed strains are independent of 11 higher approximation modes from expressions (33). This provides a correct rank of the elemental matrix [3,8]. It should be mentioned that all matrix calculations are evaluated by using the full exact analytical integration. So, our FE formulation is very economical and efficient.

Eliminating further strains and stress resultants from Eq. (35) and introducing matrices of order 11×11

$$\mathbf{D}^{r_1 r_2} = \mathbf{Q}^{r_1 r_2} (\mathbf{Q}^{r_1 r_2})^{\mathrm{T}} \mathbf{D} \mathbf{Q}^{r_1 r_2} (\mathbf{Q}^{r_1 r_2})^{\mathrm{T}},$$

one obtains the governing equilibrium equations

$$\mathbf{G}(\mathbf{V}) = \mathbf{F}, \tag{37a}$$

where

$$\mathbf{G}(\mathbf{V}) = \sum_{r_1,r_2} \frac{1}{3^{r_1+r_2}} (\mathbf{B}^{r_1 r_2} + 2\mathbf{A}^{r_1 r_2}\mathbf{V})^{\mathrm{T}} \mathbf{D}^{r_1 r_2} \times (\mathbf{B}^{r_1 r_2} + \mathbf{A}^{r_1 r_2}\mathbf{V})\mathbf{V}. \quad (37b)$$

Due to the existence of non-linear terms in Eq. (37), the Newton–Raphson iteration scheme may be employed to solve these equations

$$\mathbf{V}^{[n+1]} = \mathbf{V}^{[n]} + \left[\frac{\partial \mathbf{G}}{\partial \mathbf{V}}(\mathbf{V}^{[n]})\right]^{-1} [\mathbf{F} - \mathbf{G}(\mathbf{V}^{[n]})], \quad (38)$$

where the superscript n indicates a number of iterations.

Equilibrium equation (38) for each element are assembled by the usual technique to form the global equilibrium equations. These equations should be performed until the required accuracy of the solution can be obtained. The convergence criterion used herein can be described as

$$\|\mathbf{U}^{[n+1]} - \mathbf{U}^{[n]}\| < \varepsilon \|\mathbf{U}^{[n]}\|, \quad (39)$$

where $\| \bullet \|$ stands for the Euclidean norm in the displacement space; $\mathbf{U}$ is the global displacement vector; ε is the a priori chosen tolerance.

8. Numerical tests

Five tests concerning homogeneous and composite beams and plates undergoing finite displacements and finite rotations were employed to assess the accuracy and effectiveness of the developed 4-node plate elements. The first element TMS4c, based on the complete constitutive law (18), (23) and (24), is too stiff and its application for the bending dominated plate problems needs great care. While the second element TMS4r, based on refined constitutive laws (20)–(24), overcomes Poisson thickness-locking phenomenon that may be appreciated very much for the 6-parameter plate formulation. It should be mentioned that no difference between TMS4r and TMS4c elements can be observed when Poisson's ratios are equal to zero.

In all tests the tolerance error ε from criterion (39) is set to be $\varepsilon = 10^{-6}$. Note also that computations were performed on a standard PC Pentium/1000 using Delphi environment.

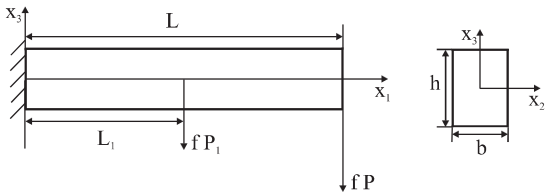

$E=3\times10^7$, $\nu=0.3$, $L_1=52.03$, $L=102.75$, $h=\sqrt{10}$
$b=\sqrt{10}/50$, $P_1=850$, $P=1350$

Fig. 4. Cantilever beam under two concentrated loads.

8.1. Cantilever beam under two concentrated loads

We consider first a cantilever beam subjected to two conservative concentrated loads as shown in Fig. 4. This is a typical beam problem with large shearing and has been frequently used for numerical testing of non-linear elements [16,27,28]. The cantilever beam has a rectangular cross section, and its mechanical and geometrical characteristics are given in Fig. 4.

Table 1 lists a comparison with the results obtained in [16] without the thickness change by using 20×1 meshes of the 8-node 2-D and 3-D plate elements with 2×2 numerical Gauss integration scheme. While we used 40×1 meshes of the TMS4r and TMS4c elements with the exact analytical integration. It is seen that all elements perform well but our TMS4r and TMS4c elements are less expensive. Note that our results have been obtained by using *only one* loading step including the last level of loading $f = 4$ and further loading is possible. In this problem we did not discover an escape of the initial guess (a result of solving the geometrically linear problem) from Newton's attraction area for all reasonable levels of loading. As it turned out, applying the non-uniform meshes improve a solution of this problem. So, the best results are derived discretizing the left and right parts of a beam by 30 and 10 elements, respectively. In this case the converged solution is achieved with 14 iterations for the loading factor $f = 4$.

The results listed in Table 1 additionally illustrate the sensitivity of the discussed non-linear plate elements to Poisson thickness locking. As already said, Poisson thickness locking occurs in bending dominated plate problems when Poisson's ratio is not equal to zero. One can see that our TMS4r element and the 2-D plate element [16] are completely free from

Table 1
Tip displacements $\bar{v}_i = (v_i^- + v_i^+)/2$ of the cantilever beam under two concentrated loads

Loading factor f	$-\bar{v}_1$				$-\bar{v}_3$			
	TMS4c element	TMS4r element	3-D plate [16]	2-D plate [16]	TMS4c element	TMS4r element	3-D plate [16]	2-D plate [16]
1	28.07	30.80	28.02	30.73	64.49	67.00	64.44	66.94
2	48.02	50.67	47.91	50.54	79.31	80.82	79.24	80.74
4	65.08	67.09			87.71	88.56		

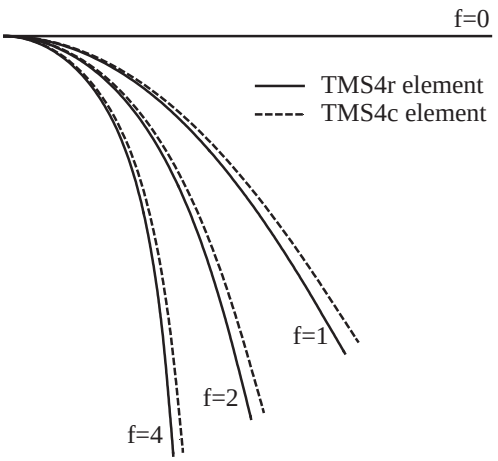

Fig. 5. Deformed configurations of the cantilever beam under two concentrated loads.

Poisson thickness locking while our TMS4c element as well as the 3-D plate element [16] are too stiff [27,28].

For the complete picture, Fig. 5 presents deformed beam configurations obtained by using both developed elements. It is seen that applying the TMS4c element for solving the non-linear bending dominated plate problems needs to be substantiated.

8.2. Cantilever plate under concentrated load at one corner

The cantilever rectangular plate depicted in Fig. 6 is subjected to the conservative transverse load at the free end. The geometrical and material data of the problem from [29,30] are shown in Fig. 6. Fig. 7 displays the results (without the thickness change) reported in [30] applying five equal load increments

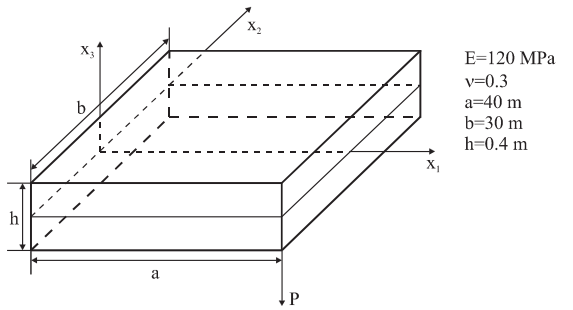

Fig. 6. Cantilever plate under a concentrated load at one corner.

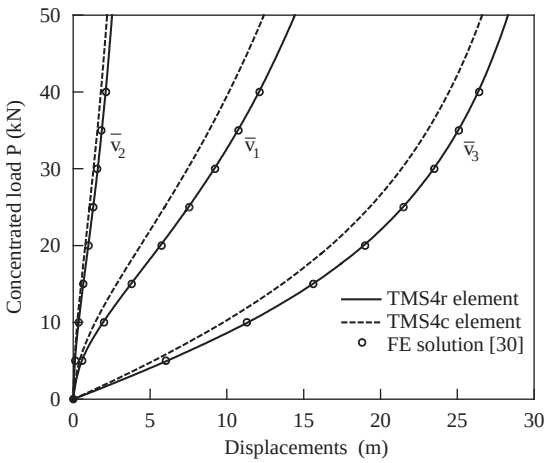

Fig. 7. Displacements of the middle plane $\bar{v}_i = (v_i^- + v_i^+)/2$ at the corner of the plate under a concentrated load at the same corner.

and our results obtained by using 8×6 meshes of the TMS4r and TMS4c elements. It is seen that our TMS4r element overcomes Poisson thickness-locking excellently while the TMS4c element is too stiff.

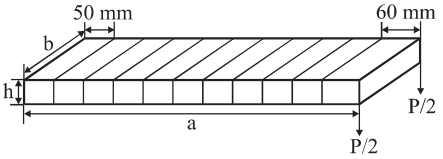

E_L=142 GPa, E_T=9.8 GPa, G_{LT}=6 GPa, G_{TT}=3.63 GPa
ν_{LT}=0.3, ν_{TT}=0.35, a=560 mm, b=30 mm, h=0.744 mm
Ply thickness=0.124 mm, Number of layers=6

Fig. 8. Cantilever narrow cross-ply plate under a concentrated load at the tip.

It should be noted that all our results have been obtained by using *only one* loading step and further loading is possible. And in this problem a choice of the solution of the geometrically linear problem as an initial guess for the Newton–Raphson method is quite enough for both developed elements and for all reasonable levels of loading including $P=200$ kN and more.

8.3. Cantilever narrow cross-ply plate under concentrated tip load

This problem was presented in [31] and further has been used as a benchmark test for non-linear orthotropic structure behaviour by Pai et al. [32]. The geometrical and material characteristics of the 6-layer narrow plate are given in Fig. 8. The cross-ply plates having ply orientations $[0/90]_3$, $[0_3/90_3]$ and $[0_2/90/0/90_2]$ are discretized using 11 TMS4r and TMS4c elements, namely, 10 elements of the equal (50 mm) lengths and a tip element of the 60 mm length (see Fig. 8). Fig. 9 presents the dependence of displacements at the point $x_1 = 500$ mm of the middle plane on the conservative concentrated load P for the $[0/90]_3$ plate. It is seen that our FE solution agrees closely with the experimental results of Minguet and Dugundji [31] and numerical results [32]. As it turned out, there is a negligible difference between the results obtained by using the TMS4r and TMS4c elements. So, Poisson's effect in the thickness direction has little meaning for this composite plate.

Additionally, Fig. 10 shows load–displacement curves for the tip points of the middle plane. Three different ply-orientations were used. As can be seen, there exists a strong dependence of the plate stiffness on the ply orientations for the extremely high level of loading.

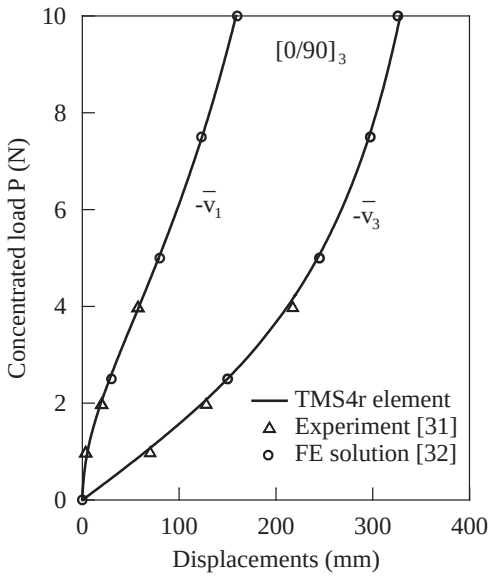

Fig. 9. Displacements $\bar{v}_i = (v_i^- + v_i^+)/2$ at $x_1 = 500$ mm of the cantilever narrow cross-ply plate under a concentrated load at the tip.

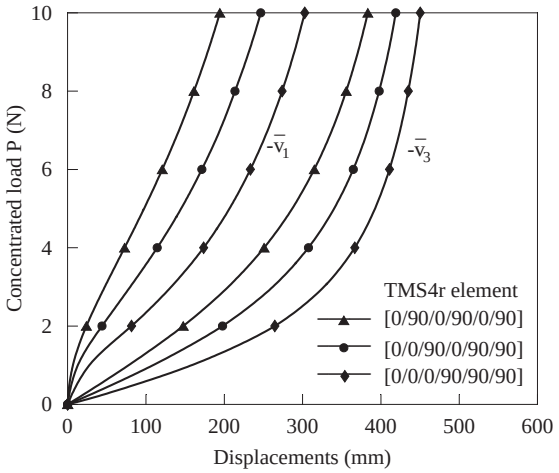

Fig. 10. Displacements $\bar{v}_i = (v_i^- + v_i^+)/2$ at $x_1 = 560$ mm of the cantilever narrow cross-ply plate under a concentrated load at the tip.

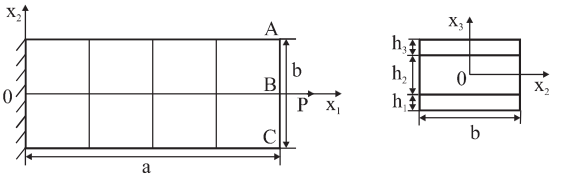

$E_L^{(1)}=E_L^{(3)}=211$GPa, $G_{LT}^{(1)}=G_{LT}^{(3)}=G_{TT}^{(1)}=G_{TT}^{(3)}=2.64$GPa
$E_T^{(1)}=E_T^{(3)}=5.27$GPa, $\nu_{LT}^{(1)}=\nu_{LT}^{(3)}=0.25$, $\nu_{TT}^{(1)}=\nu_{TT}^{(3)}=0$
$E_L^{(2)}=E_T^{(2)}=0.5$GPa, $G_{LT}^{(2)}=G_{TT}^{(2)}=0.25$GPa, $\nu_{LT}^{(2)}=\nu_{TT}^{(2)}=0$
a=2000 mm, b=800 mm, $h_1=h_3=4$ mm, $h_2=32$ mm
Ply orientation=[30/0/-30]

Fig. 11. Cantilever angle-ply sandwich plate under a concentrated tension load.

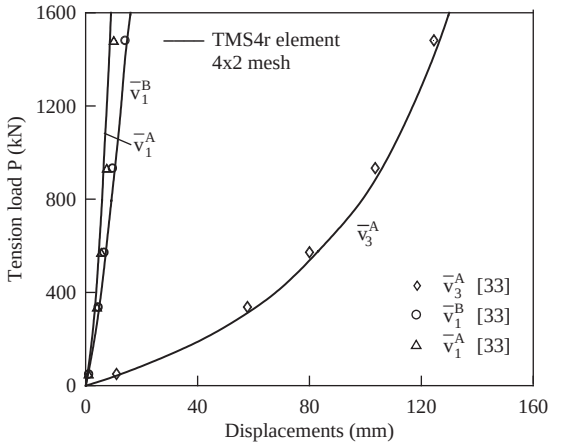

Fig. 12. Displacements $\bar{v}_i=(v_i^- + v_i^+)/2$ at the tip of the cantilever angle-ply sandwich plate under a concentrated tension load.

8.4. Cantilever sandwich angle-ply plate under concentrated tension load

The cantilever rectangular sandwich angle-ply plate is subjected to a tension load applied at the middle point of the free end as shown in Fig. 11. This problem has been treated by Rothert and Dehmel [33] for numerical testing the non-linear anisotropic plate element behaviour. The geometrical and material data of the sandwich plate [33,34] are given in Fig. 11. Due to the anisotropic plate response, we did not adopt symmetry conditions as in [34] and modeled the whole plate by using regular meshes of TMS4r elements. In Fig. 12, the load–displacement curves are compared with those reported in [33] without the thickness

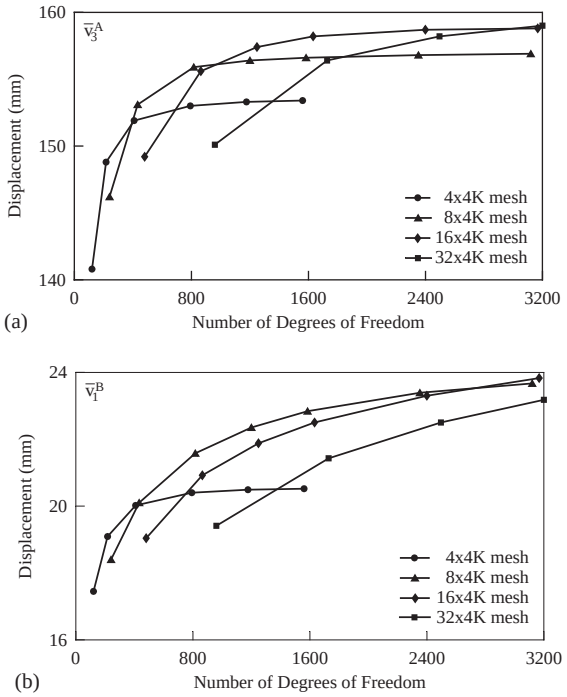

Fig. 13. Displacements (a) $\bar{v}_3^A$ and (b) $\bar{v}_1^B$ at the tip of the cantilever angle-ply sandwich plate under a concentrated load $P=1600$ kN.

change using 4×2 mesh of 4-node elements. It is seen that the concentrated tension load causes warping because there are large transverse displacements $\bar{v}_3^A$ and $\bar{v}_3^C$ at the points A and C, respectively.

For the complete picture, Fig. 13 illustrates the convergence study. And in this problem there is a negligible difference between the developed TMS4r and TMS4c elements.

8.5. Cantilever plate under two couples of tip forces

Finally, we consider a cantilever square plate subjected to two couples of forces at the free end as shown in Fig. 14. It is selected in order to test the effect of warping on the performance of the TMS4r and TMS4c elements. The geometrical and material characteristics of the plate are given in Fig. 14. The displacements of the middle plane at the corner A are presented in Fig. 15. Table 2 lists the results of convergence for different regular meshes chosen for the whole plate because no symmetry conditions were used. Note that

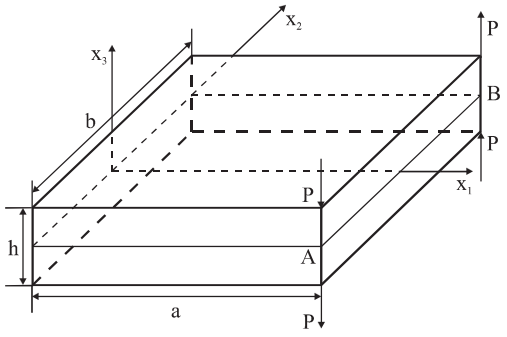

E=2×10^6, ν=0.3, a=100, b=100, h=1, P=1750f

Fig. 14. Cantilever plate under two couples of tip forces.

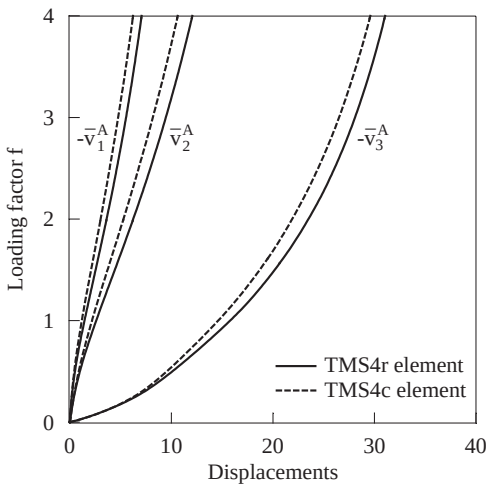

Fig. 15. Displacements $\bar{v}_i = (v_i^- + v_i^+)/2$ at the corner A of the cantilever plate under two couples of tip forces.

all results have been obtained by using again *only one* loading step and further loading is possible.

9. Conclusions

The simple and efficient FE model has been developed for the analysis of multilayered plates undergoing finite deformations. The FE formulation is based on the non-linear strain–displacement relationships that exactly represent the arbitrarily large rigid-body motions. As fundamental unknowns six displacements and 11 strains of the face planes, and 11 stress resultants have been chosen. This allows special loading conditions at the face planes and plate edges as in Section 8.5 to be accounted for.

The proposed plate theory is free of assumptions of small displacements, small rotations, small strains and small loading steps because in this paper the *exact* theory based on the fully non-linear strain–displacement relationships has been developed. As a result, the simplest quadrilateral 4-node plate element on the basis of the assumed strain concept can be used without additional stabilization algorithms. The element characteristics arrays have been obtained by applying the Hu–Washizu mixed variational principle in conjunction with the total Lagrangian formulation and Newton–Raphson method.

All matrix calculations are evaluated using the full exact analytical integration. So, our FE formulation is sufficiently economical and efficient. The developed elements do not contain any spurious zero energy modes and possess proper ranks. An important feature of our formulation is that no enhanced strains are needed to obtain the computationally exact solutions

Table 2
Displacements $\bar{v}_i = (v_i^- + v_i^+)/2$ at the corner A of the cantilever plate under two couples of tip forces using the TMS4r element

Loading factor f	Mesh	$-\bar{v}_1^A$	$\bar{v}_2^A$	$-\bar{v}_3^A$	Number of iterations
2	10 × 10	3.286	5.719	22.60	22
2	20 × 20	3.616	6.238	23.52	23
2	30 × 30	3.691	6.352	23.72	22
4	10 × 10	6.520	11.21	30.05	25
4	20 × 20	7.058	12.05	31.05	24
4	30 × 30	7.180	12.23	31.26	30

of the bending dominated plate problems and no Poisson thickness locking can occur when one uses our TMS4r element.

To demonstrate the accuracy and efficiency of the proposed elements, five tests for isotropic and composite beams and plates under conservative loading were employed. In all problems TMS4r element exhibited excellent performance. It is important that our results were obtained by using *only one* loading step for the extremely large displacements and rotations, and further loading is possible.

References

[1] D.J. Dawe, Rigid-body motions and strain–displacement equations of curved shell finite elements, Int. J. Mech. Sci. 14 (1972) 569–578.

[2] G.M. Kulikov, S.V. Plotnikova, Efficient mixed Timoshenko–Mindlin shell elements, Int. J. Numer. Methods Eng. 55 (2002) 1167–1183.

[3] G.M. Kulikov, S.V. Plotnikova, Simple and effective elements based upon Timoshenko–Mindlin shell theory, Comput. Methods Appl. Mech. Eng. 191 (2002) 1173–1187.

[4] A.K. Noor, W.S. Burton, Assessment of shear deformation theories for multilayered composite plates, Appl. Mech. Rev. 42 (1) (1989) 1–12.

[5] D.H. Hodges, A.R. Atilgan, D.A. Danielson, A geometrically nonlinear theory of elastic plates, Trans. ASME J. Appl. Mech. 60 (1993) 109–116.

[6] G.M. Kulikov, Refined global approximation theory of multilayered plates and shells, J. Eng. Mech. 127 (2001) 119–125.

[7] G.M. Kulikov, Analysis of initially stressed multilayered shells, Int. J. Solids Struct. 38 (2001) 4535–4555.

[8] G.M. Kulikov, S.V. Plotnikova, Finite element formulation of straight composite beams undergoing finite rotations, Trans. Tambov State Tech. Univ. 7 (2001) 617–633.

[9] G.M. Kulikov, S.V. Plotnikova, Investigation of locally loaded multilayered shells by mixed finite-element method. Part 1. Geometrically linear statement, Mech. Compos. Mater. 38 (2002) 397–406;
G.M. Kulikov, S.V. Plotnikova, Investigation of locally loaded multilayered shells by mixed finite-element method. Part 2. Geometrically nonlinear statement, Mech. Compos. Mater. 38 (2002) 539–546.

[10] H. Parisch, A continuum-based shell theory for non-linear applications, Int. J. Numer. Methods Eng. 38 (1995) 1855–1883.

[11] H.C. Park, C. Cho, S.W. Lee, An efficient assumed strain element model with six DOF per node for geometrically non-linear shell, Int. J. Numer. Methods Eng. 38 (1995) 4101–4122.

[12] K.J. Bathe, Finite Element Procedures, Prentice-Hall, Englewood Cliffs, NJ, 1996.

[13] P. Betsch, E. Stein, An assumed strain approach avoiding artificial thickness straining for a nonlinear 4-node shell element, Commun. Numer. Methods Eng. 11 (1995) 899–909.

[14] N. Büchter, E. Ramm, Shell theory versus degeneration—a comparison in large rotation finite element analysis, Int. J. Numer. Methods Eng. 34 (1992) 39–59.

[15] I. Kreja, R. Schmidt, J.N. Reddy, Finite elements based on a first-order shear deformation moderate rotation shell theory with applications to the analysis of composite structures, Int. J. Non-Linear Mech. 32 (1997) 1123–1142.

[16] M. Li, F. Zhan, The finite deformation theory for beam, plate and shell. Part IV. The FE formulation of Mindlin plate and shell based on Green–Lagrangian strain, Comput. Methods Appl. Mech. Eng. 182 (2000) 187–203.

[17] A.F. Palmerio, J.N. Reddy, R. Schmidt, On a moderate rotation theory of elastic anisotropic shells. Part I. Theory, Int. J. Non-Linear Mech. 25 (1990) 687–700;
A.F. Palmerio, J.N. Reddy, R. Schmidt, On a moderate rotation theory of elastic anisotropic shells. Part II. FE analysis, Int. J. Non-Linear Mech. 25 (1990) 701–714.

[18] J.C. Simo, M.S. Rifai, D.D. Fox, On a stress resultant geometrically exact shell model. Part IV. Variable thickness shells with through-the-thickness stretching, Comput. Methods Appl. Mech. Eng. 81 (1990) 91–126.

[19] L. Vu-Quoc, H. Deng, X. Tan, Geometrically exact sandwich shells: the static case, Comput. Methods Appl. Mech. Eng. 189 (2000) 167–203.

[20] T.J.R. Hughes, T.E. Tezduyar, Finite elements based upon Mindlin plate theory with particular reference to the four-node bilinear isoparametric element, Trans. ASME J. Appl. Mech. 48 (1981) 587–596.

[21] G. Wempner, D. Talaslidis, C.M. Hwang, A simple and efficient approximation of shell via finite quadrilateral elements, Trans. ASME J. Appl. Mech. 49 (1982) 115–120.

[22] Y. Basar, M. Itskov, A. Eckstein, Composite laminates: nonlinear interlaminar stress analysis by multi-layer shell elements, Comput. Methods Appl. Mech. Eng. 185 (2000) 367–397.

[23] M. Bischoff, E. Ramm, On the physical significance of higher order kinematic and static variables in a three-dimensional shell formulation, Int. J. Solids Struct. 37 (2000) 6933–6960.

[24] S. Klinkel, F. Gruttmann, W. Wagner, A continuum based three-dimensional shell element for laminated structures, Comput. Struct. 71 (1999) 43–62.

[25] G.M. Kulikov, Non-linear analysis of multilayered shells under initial stress, Int. J. Non-Linear Mech. 36 (2001) 323–334.

[26] K. Washizu, Variational Methods in Elasticity and Plasticity, 3rd Edition, Pergamon Press, Oxford, 1982.

[27] L.A. Crivelli, et al., A three-dimensional non-linear Timoshenko beam based on the core-congruential formulation, Int. J. Numer. Methods Eng. 36 (1993) 3647–3673.

[28] M. Li, The finite deformation theory for beam, plate and shell. Part I. The two-dimensional beam theory, Comput. Methods Appl. Mech. Eng. 146 (1997) 53–63.

[29] K.M. Hsiao, Nonlinear analysis of general shell structures by flat triangular elements, Comput. Struct. 25 (1987) 665–675.
[30] A. Barut, E. Madenci, A. Tessler, Nonlinear analysis of laminates through a Mindlin-type shear deformable shallow shell element, Comput. Methods Appl. Mech. Eng. 143 (1997) 155–173.
[31] P. Minguet, J. Dugundji, Experiments and analysis for composite blades under large deflections. Part I. Static Behavior, AIAA J. 28 (1990) 1573–1579.
[32] P.F. Pai, T.J. Anderson, E.A. Wheater, Large-deformation tests and total-Lagrangian finite-element analyses of flexible beams, Int. J. Solids Struct. 37 (2000) 2951–2980.
[33] H. Rothert, W. Dehmel, Nonlinear analysis of isotropic, orthotropic and laminated plates and shells, Comput. Methods Appl. Mech. Eng. 64 (1987) 429–446.
[34] C.W.S. To, B. Wang, Hybrid strain based geometrically nonlinear laminated composite triangular shell finite elements, Finite Elements Anal. Des. 33 (1999) 83–124.